Int. J. Electrochem. Sci., 11 **(2016)** 4136 - 4148

International Journal of ELECTROCHEMICAL SCIENCE
www.electrochemsci.org

Optimized In-vitro Corrosion Assessment of a FeAl intermetallic Compound Modified with Ag in Artificial Human Media

E. Sarmiento-Bustos[1], *R. A. Rodríguez-Diaz*[2,4,*], *J. Colín*[3], *A. Molina-Ocampo*[4], *S. Gaona-Jiménez*[2], *L. A. Bahena-Medina*[2].

[1] Universidad Tecnológica Emiliano Zapata del Estado de Morelos, Av. Universidad Tecnológica No. 1, Col. Palo Escrito, C. P. 62760, Emiliano Zapata, Morelos, México.
[2] Universidad Politécnica del Estado de Morelos, Boulevard Cuauhnáhuac 566, Col. Lomas del Texcal, 62574 Jiutepec, Morelos México.
[3] Facultad de Ciencias Químicas e Ingeniería, Universidad Autónoma del Estado de Morelos, Av. Universidad 1001, 62209, Cuernavaca, Morelos, México.
[4] Centro de Investigación en Ingeniería y Ciencias Aplicadas – (IICBA), Universidad Autónoma del Estado de Morelos, Av. Universidad 1001, 62209, Cuernavaca, Morelos, México.
[*]E-mail: rdiaz.unam@gmail.com

Received: 16 January 2016 / *Accepted:* 7 March 2016 / *Published:* 1 April 2016

This article presents an assessment about the effect of the addition of silver on the corrosion performance of the intermetallic alloy Fe40Al (at. %) in a biomimetic environment that simulates the biological human body fluid. In the present work, an in-vitro corrosion assessment of Fe40Al based alloys was performed, since the electrochemical parameters of Fe40Al and Fe40Al2.5Ag alloys were compared. According to the polarization curves, the corrosion current density of Fe40Al2.5Ag alloy resulted minor than that of binary Fe40Al alloy; however, according to the measurements of the linear polarization resistance, the current density of the ternary alloy resulted higher than that of the binary FeAl based alloy. This behavior is ascribed to the enhancement of the protective character of the Al-oxide layer of the Fe40Al aluminide, while the exposed time in the Hanks´ solution had elapsed.

Keywords: Corrosion, Fe-Al alloy, Hanks´ solution, biomaterial, noise, polarization curve.

1. INTRODUCTION

Nowadays, the requirement of metallic materials to be applied as biomaterials is enormous. The good properties such as elasticity, toughness, rigidity and electrical conductivity enables the metals and

doi: 10.20964/110377

alloys to be applied as biomedical materials. Typically, metals and alloys are essential and appropriate to be used as orthopedic implants, bone plates, bone fixators, artificial joints, external fixators, etc. [1] since these materials may substitute the function and performance of hard tissues in orthopedics. In dentistry, metals are used for restorations, orthodontic wires, brackets and crowns for single tooth restorations, partial dentures, retainers and dental implants [2].

Biomaterials are utilized in medical devices which interacts with biological systems. Biocompatibility is their capability to perform with appropriate response in a specific application for a host. Some examples of "appropriate responses" include resistance to blood clothing, resistance to bacterial colonization and normal healing. A very important property considered in biocompatibility includes the affinity for cells, because biomaterials are always adjacent to living tissue [3].

The corrosion performance of metallic materials to be used in biomedical applications usually is the most significant property because of biocompatibility and cytotoxicity of the products generated by the corrosion process [4]. Corrosion is a continuous and simultaneous electrochemical process which is developed on the surface of the metallic biomaterial and produces the release of metal ions and their oxides into the surrounding biological media. The liberation of elements can generate discoloration of adjacent soft tissues and allergic reactions in susceptible patients [5].

The intermetallic compounds based on aluminides of transition metals like Ni, Fe, Ti, Nb, Co, and Ti are among the materials that can function properly as structural compounds, since the Aluminum content of these kind of compounds cause the generation of a passive layer of Al_2O_3, which is responsible of a good oxidation, corrosion and sulfidation resistance in a wide range of temperatures. Also, these intermetallic compounds retain strength and stiffness at elevated temperatures [6, 7].

Iron aluminide compounds are being subject of considerable attention relative to its aqueous corrosion properties. Their corrosion behavior has been investigated in a wide range of electrolytes such as acidic, basic, chloride and sulphur-compound solutions [8-11]. These compounds can be considered as potential biomaterials in room temperature or seawater atmosphere applications.

It is not possible to execute corrosion tests on these metallic implants by the typical weight loss method since their rate of corrosion is extremely small and usually this kind of tests require a long time to obtain practical results. Thus, in corrosion studies of these alloys exposed to the biomimetic physiological solution, the electrochemical techniques are more appropriate [12-14].

Therefore, the main purpose of this work is to investigate and evaluate the effect of alloying Ag to the intermetallic Fe40Al on its corrosion behavior when exposed to Hanks´ Solution by means of electrochemical techniques.

2. MATERIALS AND METHODS

2.1 Materials

The binary Fe40 Al (at. %) and ternary Fe40Al2.5 Ag (at. %) alloys were elaborated using vacuum induction furnace. Hereafter these alloys are named as Fe40Al and Fe40Al2.5Ag. The purity of the starting elements Fe, Al and Ag was equal to 99.9 %. Fe, Al and Ag were put inside in a SiC crucible in order to melt the metallic elements. The molten Fe-40Al, Fe40Al2.5Ag alloys were

discharged into a rectangular steel mold in order to obtain a microstructure with grain sizes of the order of few hundreds of microns.

2.2 Specimens preparation

The metallic electrodes were prepared by polyester resin mounting of alloys, leaving areas for exposure to the electrolytic media from 0.5 to 1.0 cm^2. The surfaces exposed to the corrosive electrolyte were prepared by sequential grinding with SiC paper up to #1500 finishing. After, the samples were mechanically polished with 1 μm alumina slurry.

2.3 Procedure for Electrochemical Tests

As electrolytic medium, the Hank solution was used, its composition is shown in the Table 1.

Table 1. Chemical composition of the Hank's solution

Compound	NaCl	$CaCl_2$	KCl	Glucose	$NaHCO_3$	$MgCl_2.6H_2O$	$Na_2HPO_4.2H_2O$	KH_2PO_4	$MgSO_47H_2O$
g/l	8	0.14	0.4	1	0.35	1	0.06	0.06	0.06

A three electrode cell configuration was utilized for the electrochemical measurements, for these experiments as saturated calomel reference electrode (SCE) as reference electrode and a graphite bar as the auxiliary electrode. All tests were developed at 30 ± 1 °C. The corrosion test were performed by means of the following electrochemical techniques: Potentiodynamic Polarization Measurements, Electrochemical Noise (EN) and Linear Polarization Resistance (LPR).

Potentiodynamic polarization scans were performed with a scan rate of (1 mV/s), in the interval from -1000 mV SCE up to +1000 mV SCE.

Electrochemical noise scans were developed using a set-up in electrochemical noise (EN) mode. Two identical samples were utilized as the working electrodes and a saturated calomel reference electrode (SCE) respectively. Each set of EN records, containing 1024 data points, at a sample rate of one point per second.

For obtaining the LPR data, the samples were polarized at ± 10 mV with respect to the free corrosion potential E_{corr}, at a scan rate of 1 mV/s during 30 days.

The Open Circuit Potential (OCP) was measured and registered while the exposure time had elapsed during 30 days. For these measurements, a three electrode cell configuration was utilized.

2.4 Microestructural characterization

The microestructural characteristics of samples were analyzed by using the Scanning Electron Microscopy (SEM). In addition, the X ray diffraction technique was utilized in order to characterize the crystal structures and phases contained in the samples.

The X-ray diffractometer was utilized, using Cu tube (K_α line radiation: $\lambda = 0.15406$ nm). The XRD spectra were recorded in the 2θ range from 20 to 80° (with step size 0.02, time per step 0.6 s).

3. RESULTS AND DISCUSSION

3.1 Microestructural characterization un-corroded specimens

The microstructural features of the as-cast Fe40Al intermetallic compound is displayed in Figures 1(a) and 1(b) which presents the macro-structure of the binary intermetallic compound exhibiting a chill-type grains morphology constituted by chill, equiaxial and columnar grains. In this micrograph, the macro-grains exhibit sizes from fractions of millimeter to more than 1 mm. The XRD, SEM and Chemical Analyses performed on surface of the binary Fe40Al alloy did not reveal the presence of precipitates or any possible segregation. This finding is in agreement with the interval of composition 35-50 (at. %) Al, which contains a FeAl phase with a B2-type crystalline structure, as is indicated in the phase diagram for the Fe-Al system [15]. The Fe40Al intermetallic compound displays that the mean size of chill morphology grains was 276 ± 88 μm, the dimensions of the columnar grains were 280 ± 94 μm in width and 2200 ± 130 μm in length and the size of equiaxial morphology grains was 548 ± 91 μm.

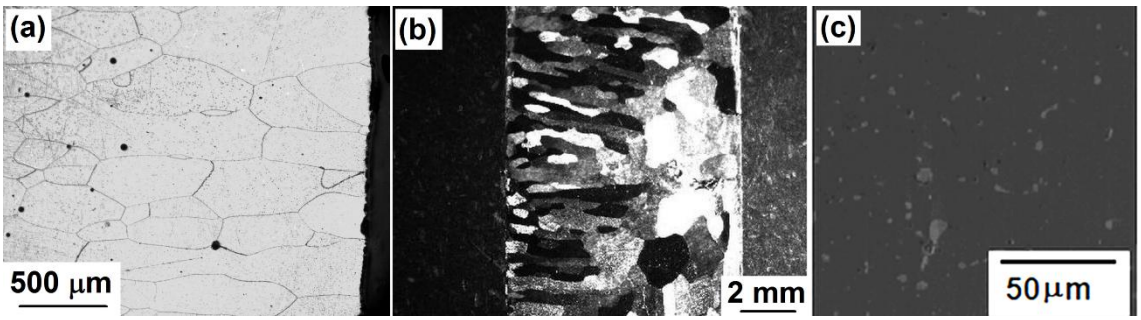

Figure 1. As-cast alloys a) Microstructure of Fe40Al, b) Macrostructure of Fe40Al and c) Microstructure of Fe40Al2.5Ag.

Figure 1(c) shows the microstructure a ternary Fe40Al2.5Ag alloy, were is observed light gray precipitates with rounded morphology which are distributed inside a grain of Fe40Al alloy, according to the point chemical analyses, these light gray precipitates belong to pure Ag phase.

Also, in accordance with the binary alloy phase diagram Al-Ag, the phase δ could have been precipitated in the matrix Fe40Al [17]. This discovery indicates that FeAl matrix acting as a solvent did not dissolved the Ag solute; but rather, silver precipitated uniformly in the binary intermetallic compound. This comportment is ascribed to the null solubility of Ag in both Al and Fe elements just as is shown in the binary alloy phase diagrams of the systems Al-Ag and Fe-Ag [16, 17]. In the binary alloy phase diagram of the system Al-Ag in the corner rich in silver, there exists a phase rich in (Ag)

from 0 to 3 wt. % Al or 0 to 10 at. % Al. In this phase, diagram from 10 to 33.5 (at. %), exists a biphasic region composed by (Ag) and δ with Pearson symbol hP2 and space group $p6_3/mmc$.

3.2. Potentiodynamic polarization tests

The potentiodynamic polarization plots of Fe40Al based alloys are shown in Figure 2, where an active-passive behavior in both alloys is observed.

Table 2 shows the electrochemical parameters determined from potentiodynamic polarization test of Fe40Al alloys exposed to Hanks´ solution, where the addition of Ag turned the E_{corr} to nobler values of potential, reaching a value of -676.4 mV. While the lowest i_{corr} value corresponded to ternary Fe40Al2.5Ag alloy with i_{corr} =3.3 $x10^{-4}$ mA/cm^2. Therefore, the corrosion rate (mm/yr) of Fe40Al2.5Ag determined by this method resulted minor than that of binary Fe40Al alloy. Fe40Al alloy exhibits, a pseudo-passivation behavior which started at i_{pass}=$6x10^{-4}$ mA/cm^2. This behavior could attributed to the generation of partially protective film of corrosion products on the alloy surface. According to Pourbaix diagram represented by the Potential-pH equilibrium diagram for the system aluminum-water at 25°C and, considering values of potential of -7 V towards noble potentials and neutral pH of 7 that is typical of Hanks´ solution. Therefore, Al is within passivation zones under these thermodynamic parameters. In this case, the passive layer is constituted by $Al_2O_3.3H_2O$ [18-19].

The pseudo-passivation behavior of binary alloy ended at the pitting potential, E_{pit} of -384 mV. Fe40Al2.5Ag alloy exhibits a more defined passivation behavior which starts at a passivation potential E_{pass} of -432 mV and ends at the pitting potential, E_{pit} of -174.5 mV.

Rodríguez-Díaz *et. al.* [20] performed linear potentiodynamic tests in Fe40Al2.5Cr and Fe40Al2.5Ti under the same experimental conditions, the authors reported values of i_{corr} of $9.3x10^{-4}$ and $9.5x10^{-4}$ mA/cm^2 for Fe40Al2.5Ti and Fe40Al2.5Cr respectively. Therefore, the corrosion rate of Fe40Al2.5Ag alloy resulted lower as compared with these Fe40Al based alloys. In order to compare the electrochemical parameters, E_{corr} and i_{corr} of FeAl alloys assessed in this work with that of commercial standard biomaterials such as Ti or Stainless Steel SS316L. Arrieta Gonzalez *et. al.* [21] measured the E_{corr} and i_{corr} values of Ti and SS 316L and reported corrosion potentials of -111 mV and -198 mV respectively. In addition, the authors reported values of corrosion current density (i_{corr}) of 0.0045 mA/cm^2 and 0.00007 mA/cm^2 for Ti and SS 316L respectively. Thus, in this case, the corrosion current density of Fe40Al and Fe40Al2.5Ag studied in this work resulted minor than that of Ti, as reported previously. Previous investigations have reported that the oxide on Ti and Ti-6Al-4V when exposed to physiological solution is predominantly composed by TiO_2 with minor amounts of TiO, Ti_2O_3, or both [22-23].

Besides, the lower corrosion rate, i_{corr} exhibited by SS 316L could be ascribed to the high protectiveness of the passive layer formed on SS 316L in biomimetic solutions which are composed mainly of Cr and Fe oxides, with minor contents of Ni and Mo oxides [24].

The Tafel slopes a_{cat} and b_{anod} were determined from polarization curves and are included in table 2. In this case, the lower values of a_{cat} and b_{anod} exhibited by the ternary Fe40Al2.5Ag alloy, indicates a lower corrosion rate, just as is established in the "Stern and Geary" equation [27, 28].

Table 2. Electrochemical parameters of the Fe-Al alloys exposed to Hanks´ solution.

Composi-tion alloy	E_{corr} (mV)	i_{corr} (mA/cm^2)	E_{pit} (mV)	i_{pit} (mA/cm^2)	E_{pass} (mV)	i_{pass} (mA/cm^2)	a_{cat}	b_{anod}	Corrosion rate (mm/yr)
Fe40Al	-701.7	4.7 x 10^{-4}	-384.3	0.0021	-637.8	5.6 x 10^{-4}	184.0	549.0	0.0062
Fe40Al2.5 Ag	-676.4	3.3 x 10^{-4}	-174.5	0.028	-432	0.01	158.7	136.7	0.0045

Thus, it can be inferred that the passive film formed over SS316L is more protective than that of Ti or its alloys.

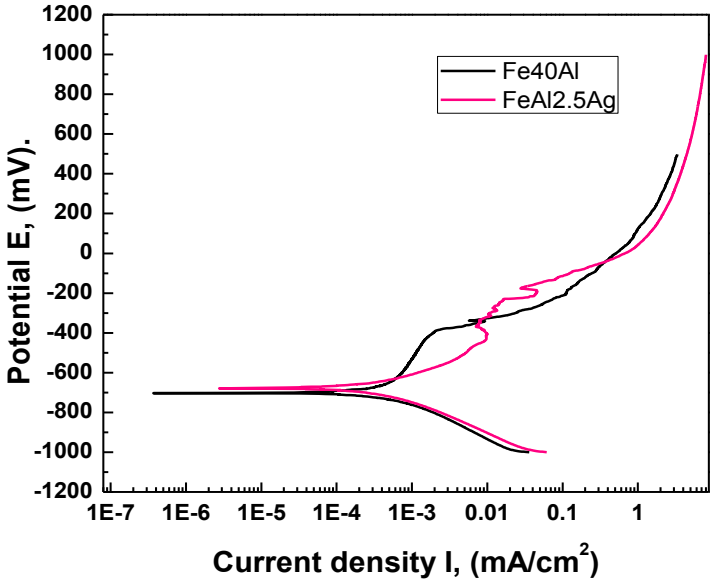

Figure 2. Potentiodynamic polarization of Fe40Al based alloys exposed to Hanks´ Solution at room temperature.

Since Fe40Al based alloys pertain to the family of intermetallic compounds named aluminides. Another important type of aluminides are the Ni-Al intermetallic compounds. Castañeda *et. al.* [25] carried out an investigation about the corrosion behavior of 50Ni-30Al-20Cu (wt. %) intermetallic alloy in a synthetic human body fluid environment by means of electrochemical techniques. The authors reported a value of i_{corr} of 6.90 x 10^{-4} mA/cm^2 for the alloy 50Ni-30Al-20Cu. In comparison, the corrosion rate expressed in terms of i_{corr} of Fe40Al based alloys studied in this work resulted minor than that Ni-Al based intermetallics. This behavior could be due to the less protective character of NiO film formed over 50Ni-30Al-20Cu intermetallic as compared with corrosion protection provided by Al-oxide formed over Fe40Al based intermetallics.

3.3. Open circuit potential (OCP) measurements.

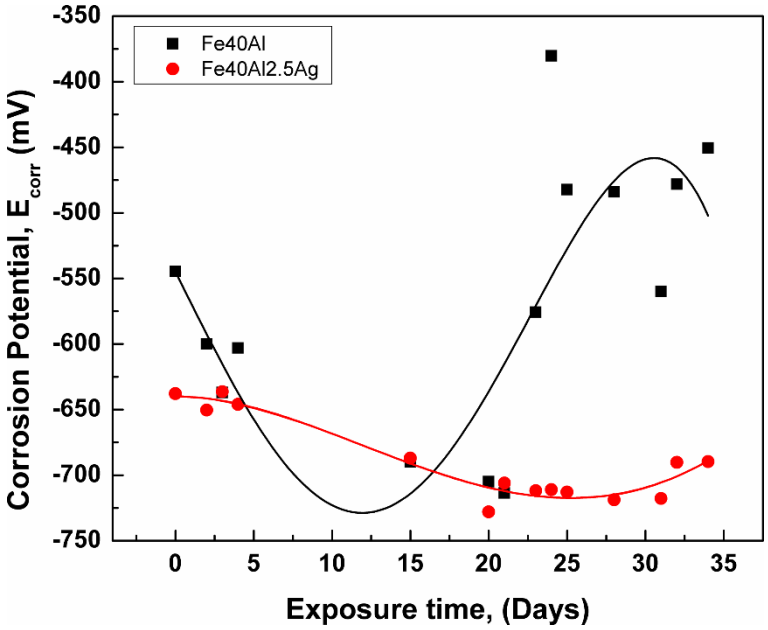

Figure 3. Variation of corrosion potential (E_{corr}) of Fe40Al based alloys as a function of exposure time

Figure 3 shows the dependence of E_{corr} with the exposure time for Fe40Al based alloys that display a diminution behavior to more negative values during the first 5 days of immersion. E_{corr} of Fe40Al2.5Ag clearly exhibited a trend to diminish while the exposure time had elapsed from day 0 to the 35th day of test. In contrast, the corrosion potential of the binary Fe40Al alloy increased as the exposure time advanced from the 5th to the 35th immersion days, this behavior is because Al based alloys, generally form a passive layer which consists mainly of Al_2O_3 [26]. Figure 3 shows that the potential corrosion of ternary Fe40Al2.5Ag alloys is minor than that of the binary intermetallic alloy. This behavior possibly is because the rich phase of silver distributed uniformly in the Fe40Al alloy decreased the protective character of the Al_2O_3 passive layer. In addition, the presence of silver together with the intermetallic phase in this alloy, suggest the formation of a galvanic couple which promoted a change of corrosion potential towards a more active direction.

3.4. Linear Polarization Resistance Measurements, R_p.

The variation of R_p as a function of exposure time, for the Fe40Al based alloys is shown in Figure 4.

The Linear Polarization Resistance value of Fe40Al and Fe40Al2.5Ag alloys displayed an erratic variation while the test time had advanced. It is suggested that this behavior can be attributed to passivation-repassivation processes. It can be observed from figure 4 that R_p values of the binary Fe40Al alloy resulted higher than those of ternary Fe40Al2.5Ag alloy. This behavior is because ternary Fe40Al2.5Ag alloy was degrading at a higher corrosion rate than the Fe40Al alloy, since R_p is inversely proportional to i_{corr}, just as is indicated in the "Stern and Geary" equation [27, 28].

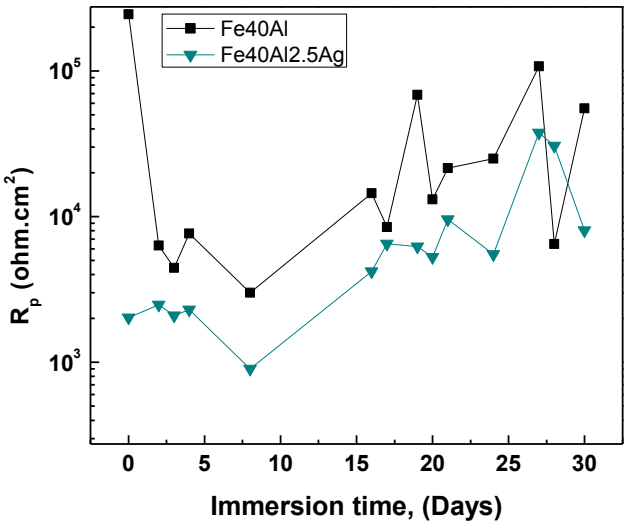

Figure 4. Dependence of Linear Polarization Resistance (R_p) of Fe40Al based alloys with exposure time in Hanks´ Solution.

Minor corrosion rate exhibited by ternary Fe40Al2.5Ag alloy compared with that of Fe40Al alloy is not congruent with the corrosion rate determined by the polarization curves. However, this behavior is due to the fact that the protective nature of the passive film formed on the surface of the binary Fe40Al alloy was improved while the immersion time had elapsed. This enhancement of protective character of Al_2O_3 layer could be attributed to the growth of its thickness, besides its porosity could have diminished.

3.5 Electrochemical Noise Measurements

The noise resistance, R_n can be obtained by dividing the standard deviation of the noise potential σ_v by the standard deviation of the noise current, σ_i. Figure 5 shows the variation of noise resistance as a function of immersion time for Fe40Al based alloy. The fluctuations of R_n values for the Fe40Al and Fe40Al2.5Ag alloys shown a drop from day 0 to day 3 in one order of magnitude. After the third day of exposition, R_n values of both alloys fluctuated, with a general tendency to increase for almost three orders of magnitude.

Fluctuating behavior of R_n values of both, binary and ternary alloys could be due to alternate processes of detachment and re-establishment of the passive layer formed on the surfaces of the intermetallic. Also, this comportment could be ascribed to the variation of the protective nature of the passive film formed during the advance of immersion time. This change of protective character of passive Al_2O_3 film could be due to a decrement of its porosity or the increase of its thickness. Since, Al alloys, when exposed to chloride solutions are susceptible to pitting corrosion process [29], then R_n variation is related to the change of the pitting corrosion resistance during the immersion experiments. This, in turn, is due to the change of the physical and chemical properties of the passive layer while the immersion time had elapsed.

The "Localization Index, IL", defined as:

$$IL = \frac{\sigma_i}{i_{rms}} \quad (1)$$

In equation 1, σ_i is the standard deviation of the noise current and i_{rms}, the root mean squared of the current noise. The IL values obtained from equation 1, are related to de kind of corrosion that the alloys had presented. When IL values lie between 0.01 and 0.001, the intermetallic presents uniform corrosion. However, when IL values are within the range of 0.1 to 0.01, the alloys are susceptible to both types of corrosion (uniform and localized), and finally, when the IL values lie between 1 and 0.1, the material is highly susceptible to localized corrosion.

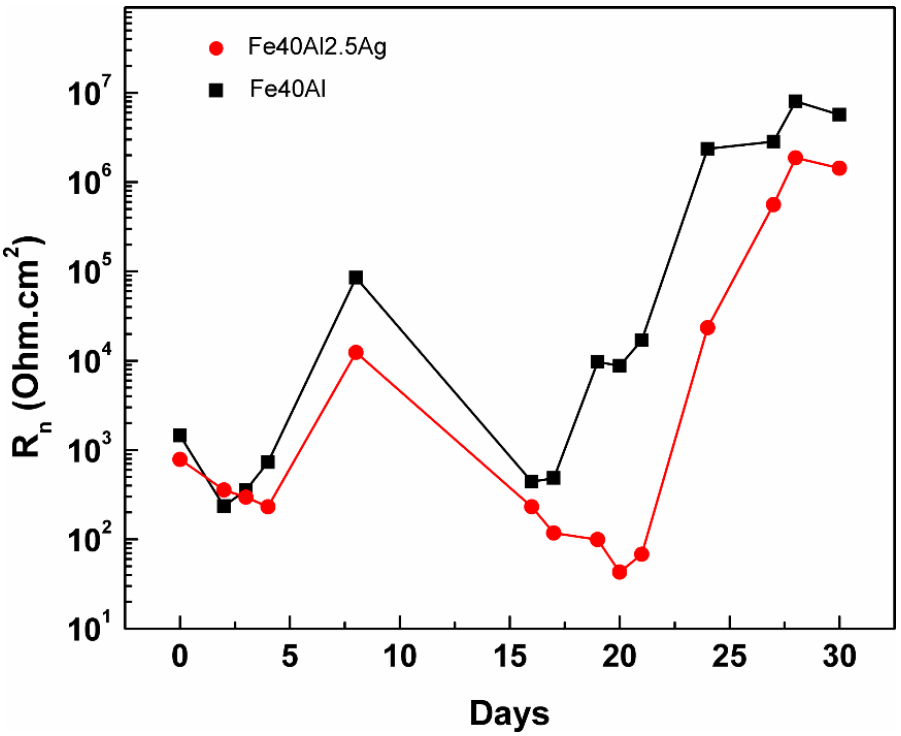

Figure 5. Dependence of the noise resistance, R_n, of the Fe40Al based alloys with exposure time in Hanks´ solution.

According to Table 3, binary and ternary intermetallic alloys experienced a mixed type of corrosion, constituted by both types of corrosion, uniform and localized during the first 15 days of immersion.

However, at the end of immersion time, binary and ternary alloys, exhibited only a uniform corrosion. This phenomena associated to the enhancement of protective nature of the passive layer formed on surface of the materials studied in present work. This strengthening of the corrosion resistance derived from the protective quality of the Al_2O_3 film, may be associated to the diminution of its porosity while the immersion time had elapsed.

Table 3. Localization Index values for the intermetallic alloys.

Alloy (at.%)	Exposure time (days)	Localization Index (IL)	Corrosion type
Fe40Al	0	0.037	Mixed*
	15	0.035	Mixed*
	30	0.001	Uniform
Fe40Al2.5Ag	0	0.046	Mixed*
	15	0.019	Mixed*
	30	0.001	Uniform

*Mixed: localized and uniform corrosion

3.6 Microstructural Characterization of Corroded Alloys

Figure 6 (a) exhibits a corroded surface of Fe40Al alloy after a period of immersion of 30 days in Hanks´ Solution. Also, Figures 6 (b) to 16 (f) display the X-ray chemical mappings of corrosion products corresponding to Fe, Al, O, Ca and C elements in a respective way. According to chemical mappings of iron and aluminum, the region whose color is bright gray corresponds to the intermetallic Fe40Al. Figure 6 (d) shows the presence of oxygen in the zone were Fe40Al is present, which is related to the presence of Al-oxide in the intermetallic surface [18, 19].

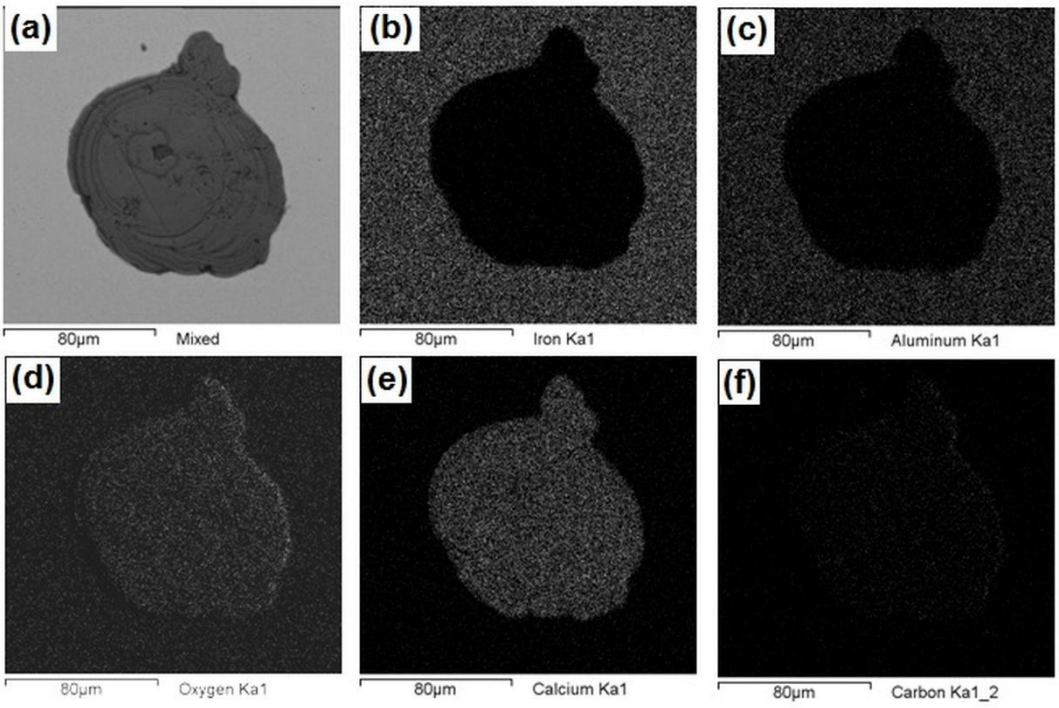

Figure 6. SEM micrographs of the corroded surface of (a) Fe40Al with the chemical mappings of (b) Fe, (c) Al, (d) O, (e) Ca and (f) C.

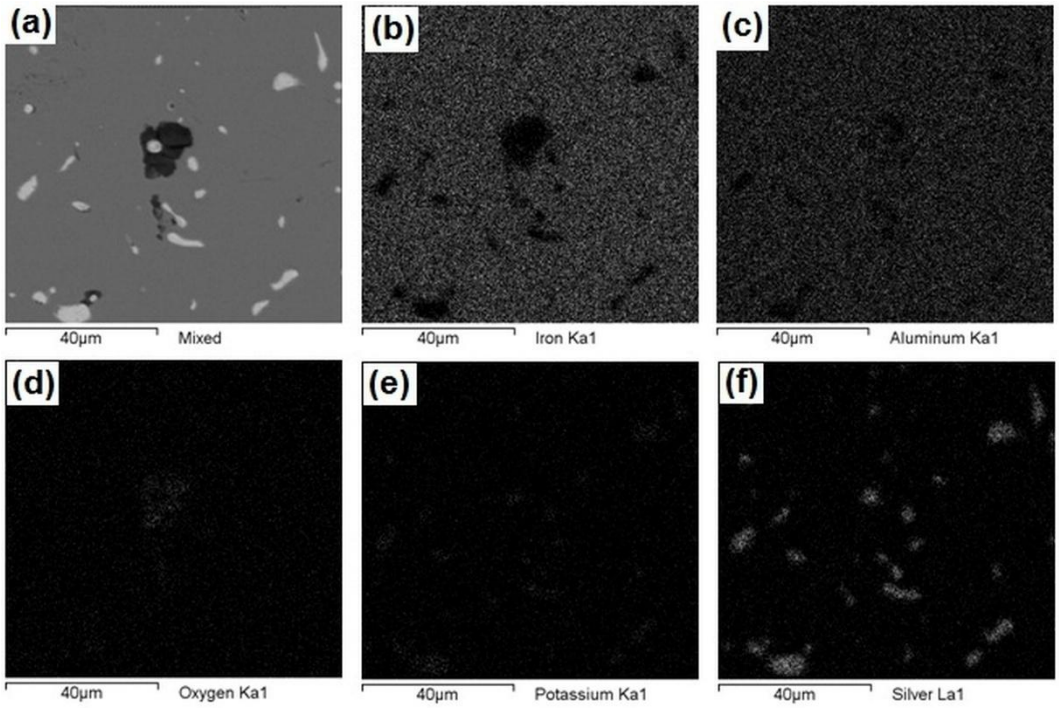

Figure 7. SEM micrographs of the corroded surface of (a) Fe40Al2.5Ag with the chemical mappings of (b) Fe, (c) Al, (d) O, (e) K and (f) Ag.

The Figures 6 (d) to 6 (f) shows the presence of O, Ca and C in a dark gray film composed of corrosion products formed on the surface of binary intermetallic alloy. The presence of these elements suggest the probable formation of $CaCO_3$ and CaO compounds. The secondary electron micrograph displayed in Figure 6 (a) shows a uniform type of corrosion, this phenomena is in accordance with the IL of the binary Fe40Al alloy that is included in Table 3. The Figures 6 (d) to 6 (f) the shows presence of O, Ca and C in a dark gray film composed of corrosion products formed on the surface of binary intermetallic alloy. The presence of these elements suggest the probable formation of $CaCO_3$ and CaO compounds. The secondary electron micrograph displayed in Figure 6 (a) shows a uniform type of corrosion, this phenomena is in accordance with the IL of the binary Fe40Al alloy that is included in Table 3.

Figure 7 shows the SEM images of the Fe40Al2.5Ag alloy together with the corresponding chemical mappings of Fe, Al, O, K and Ag. Figures 7(b), 7(c) and 7(d), indicate the existence of Fe, Al and O on the corroded alloy surface. The presence of these elements is related with the formation of Al-oxides on corrosion products.

Previous reports agree with the formation of Al_2O_3 film on the surfaces of iron aluminides [30-31].

Figure 7 (a) shows a secondary electron micrograph that exhibits bright round precipitates of a phase rich in Ag uniformly distributed in the binary Fe40Al binary matrix. In this illustration it can be observed pits with sizes ranging within the interval of values of about 2.5 to 15 µm. These pits surround the particles of silver, it is suggested that this localized type of corrosion was induced by the formation of a galvanic couple constituted by the Ag and Fe40Al phases, since under standard

conditions, the silver possess a very noble reduction potential as compared with that of Fe and Al. The secondary electron micrograph displayed in Figure 7 (a) shows a mixture uniform and localized corrosion types, which is in agreement with the IL for ternary Fe40Al2.5Ag alloy that is included in Table 3.

4. CONCLUSIONS

The corrosion nature of Fe40Al based alloys as candidate materials to be utilized as metallic implants, in the physiological body environment has been characterized. The potentiodynamic polarization plots exhibited that binary Fe40Al alloy showed the greatest corrosion resistance as compared with that of ternary alloy Fe40Al2.5Ag.

However, according to $R_{p,}$ curves, the binary alloy exhibited the highest corrosion resistance as compared with that of ternary alloy. This behavior is ascribed to the improvement of the protective nature of the Al_2O_3 layer of Fe40Al intermetallic alloy while the immersion time in the artificial biological solution had elapsed.

In accordance to electrochemical noise tests, the intermetallic alloys underwent a mixed type of corrosion, constituted by two types of corrosion, localized and uniform during the first 15 days of exposure. However, after 30 days of immersion, binary and ternary alloys exhibited only a uniform corrosion. This behavior can be attributed to the improvement of the protective character of the passive layer formed on surface of the intermetallics.

It is concluded that Fe40Al based alloys could be used as biomaterials in biological applications, since this alloys shows good corrosion performance.

ACKNOWLEDGEMENT
The authors express their gratitude to PRODEP and CONACyT for their financial support provided for the development and accomplishment of this research.

References

1. T. Hanawa, *Sci. Technol. Adv. Mater*., 3 (2002) 289
2. J.F. McCabe, A.W.G. Walls, Applied Dental Materials, Wiley-Blackwell, Oxford UK (2008)
3. Q. Chen & G.A Thouas. *Materials Science and Engineering: R: Reports*, 87 (2015) 1
4. D. Upadhyaya, M. A. Panchal, R. S. Dubey, V. K. Srivastava, *Mater. Sci. Eng*. A., 432 (2006) 1
5. T.P. Chaturvedi, *Indian Journal of Dental Research*, 20 1 (2009) 91
6. M. Zamanzade, J.R. Velayarce, O.T. Abad, C. Motz & A. Barnoush. *Materials Science and Engineering: A*, 652 (2016) 370
7. M. Zamanzade, A. Barnoush & C. Motz. *Crystals*, 6(1) (2016) 10
8. E. Huape-Padilla, M. Sánchez-Carrillo, J.P. Flores-de los Rios , M. A. Espinosa-Medina, R. G. Bautista-Margulis, M. I. Ferrer-Sánchez & A. Martínez-Villafañe. *Int. J. Electrochem. Sci*, 10 (2015) 2141

9. M. Jez, M. Mitoraj, E. Godlewska, M. Jakubowska & B. Bas. *Journal of Solid State Electrochemistry,* 18(6) (2014) 1635
10. F. Rosalbino, R. Carlini, R. Parodi, G. Zanicchi & G. Scavino. *Corrosion Science*, 85(2014) 394.
11. C. Senderowski, M. Chodala & Z Bojar. *Materials*, 8(3) (2015) 1108
12. L. Concha-Guzmán, E. Sarmiento-Bustos, C. Menchaca-Campos, J. Uruchurtu-Chavarín, OmniaScience Monographs, España (2015)
13. M. A. Ramirez-Arteaga, J. G. Gonzalez-Rodriguez, E. Sarmiento-Bustos, I. Rosales, *Int. J. Electrochem. Sci.*, 9 (2014) 161
14. C. Menchaca-Campos, E. Sarmiento-Bustos, J. Uruchurtu, *Recent Pat. Corros. Sci*., 3 (2013) 12
15. O. Kubaschewski, *Iron—Binary phase diagrams*, Springer Science & Business Media, Berlin (2013)
16. N. A. Zarkevich & D. D. Johnson. *Physical Review B*, 67(6) (2003) 064
17. H. Okamoto, Phase Diagrams of Binary Alloys, ASM International, Ohio (2010)
18. M. Pourbaix, Lectures on Electrochemical Corrosion, Springer Science & Business Media, New York (2012)
19. M. Pourbaix, *Biomaterials*, 5 (1984) 122
20. R. A. Rodríguez-Díaz, J. Uruchurtu-Chavarín, A. Molina-Ocampo, J. Porcayo-Calderón, M. González-Pérez, J. M. López-Oglesby, J. A. Juárez-Islas, *Int. J. Electrochem. Sci*, 8 (2013) 958
21. C. D. Arrieta-Gonzalez, J. Porcayo-Calderon, V. M. Salinas-Bravo, J. G. Gonzalez-Rodriguez, J. G. Chacon-Nava, *Int. J. Electrochem. Sci*, 6 (2011), 4016
22. I. Milosev, M. Metikos-Hukovic, H. H. Strehblow, *Biomaterials*, 21 (2000) 2103
23. M. A. Arenas, T. J. Tate, A. Conde, J. De Damborenea, *Br. Corros. J*., 35 (2000) 1
24. I. Milosev, H. H. Strehblow, *J. Biomed. Mater. Res*., 52 (2000) 404
25. I. E. Castañeda, J. G. Gonzalez-Rodriguez, G. Dominguez-Patiño, R. Sandoval-Jabalera, M. A. Neri-Flores, J. G. Chacon-Nava, A. Martinez-Villafañe, *Int. J. Electrochem. Sci*., 6 (2011) 404
26. F. Rosalbino, R. Carlini, R. Parodi, G. Zanicchi & G. Scavino. *Corrosion Science*, 85 (2014) 394
27. L. Luo, *Journal of The Chinese Ceramic Society*, 42(5) (2014) 574
28. F. Mansfeld,. *Journal of Solid State Electrochemistry*, *13*(4) (2009) 515
29. B. Zaid, D. Saidi, A. Benzaid, & S. Hadji C*orrosion Science*, 50(7) (2008) 1841
30. M. Zamanzade, H. Vehoff & A. Barnoush. *Acta materialia*, 69 (2014) 210
31. M. Zamanzade & A. Barnoush. *Corrosion Science*, 78 (2014) 223